Adsorption, 1, 133–151 (1995)

Sensitivity of PSA Process Performance to Input Variables

D.G. HARTZOG
Dynamic Matrix Control Corp., 9896 Bissonet, Houston, TX 77036

S. SIRCAR
Air Products and Chemicals, Inc., 7201 Hamilton Boulevard, Allentown, PA 18195-1501 USA

Received June 28, 1994; Revised October 18, 1994; Accepted October 24, 1994

Abstract. Mathematical models for pressure swing adsorption (PSA) processes essentially require the simultaneous solutions of mass, heat and momentum balance equations for each step of the process using appropriate boundary conditions for the steps. The key model input variables needed for estimating the separation performance of the process are the multicomponent adsorption equilibria, kinetics and heats of adsorption for the system of interest. A very detailed model of an adiabatic Skarstrom PSA cycle for production of high purity methane from a ethylene-methane bulk mixture is developed to study the sensitivity of the process performance to the input variables. The adsorption equilibria are described by the heterogeneous Toth model which accounts for variations of isosteric heats of adsorption of the components with adsorbate loading. A linear driving force model is used to describe the kinetics. The study shows that small errors in the heats of adsorption of the components can severely alter the overall performance of the process (methane recovery and productivity). The adsorptive mass transfer coefficients of the components also must be known fairly accurately in order to obtain precise separation performance.

Keywords: PSA process, sensitivity, equilibria, kinetics, heats

Introduction

Numerous pressure swing adsorption (PSA) processes have been designed, developed and commercialized for separation of bulk gas mixtures during the last 25 years. These processes differ by (a) the modes of operation of the adsorption, the desorption and the complementary steps used in the cyclic process, (b) the types of adsorbent used in the system, (c) the operating conditions of the process steps, and (d) the product specifications such as number of products, product purity and pressure, product recovery and quantity per cycle, etc.

It may often be necessary to mathematically model the operation of a specific PSA process of interest in order to scale-up and optimize the design. A conventional PSA model requires that the conservation partial differential equations (PDE's) describing the component mass balances, the gas and adsorbed phase heat balances, and the momentum balance within the adsorber be simultaneously solved (integrated) for each step of the cyclic PSA process using the appropriate initial and boundary conditions for the step. The final conditions (pressure, temperature, gas phase composition and adsorbate loading profiles along the length of the adsorber) within the adsorber at the end of any cyclic step becomes the initial condition at the beginning of the next sequential step and so on. These calculations are carried out over many complete cycles for the process until a cyclic steady-state performance solution is achieved. The boundary conditions for each step of the PSA cycle are determined by the process design.

The key input variables for the solution are [Sircar, 1991a]:

(a) Multicomponent adsorption equilibria
(b) Multicomponent adsorptive mass transfer characteristics
(c) Multicomponent isosteric heats of adsorption.

The quality of the PSA process simulation largely depends on the detailedness of the mathematical framework for the conservation equations, the accuracy of the integration technique used, and the accuracy of the input multicomponent adsorptive properties listed above. These properties must be adequately described under all conditions of operations of the steps of the PSA process. It is preferred that these properties be represented by analytical functions of independent variables such

as gas phase pressure, temperature and composition so that the integration process is facilitated.

Many published PSA models use simplified model frameworks (such as isothermal operation, attainment of local adsorption equilibrium, isobaric adsorption and purge steps, etc.) and elementary adsorptive properties (such as linear, Langmuirian or other homogenous adsorption isotherms, constant heats of adsorption of components, etc.) in order to get a first pass estimate of the performance of a PSA process. These models can be very useful for screening the performance of an adsorbent in a given PSA process as well as for evaluating the effects of key process variables. On the other hand, it should be emphasized that the requirements for acceptable performance of an industrial PSA process can be very rigid. Economic competition dictates that the actual performance be simulated fairly accurately. The specification for the product gas purity from a PSA process is often extremely stringent while its recovery and productivity must be known within a few percent of the desired design value.

The purpose of this paper is to analyze the sensitivity of the performance of a simple PSA process to errors in the input variables by using a very detailed non-isothermal, non-isobaric (adsorption and purge steps), and non-equilibrium model framework in conjunction with a realistic model of multicomponent adsorption equilibria and heats, suitable for describing adsorption on energetically heterogeneous adsorbents.

PSA Process and Model

The PSA process evaluated in this work is the simple four-step Skarstrom Cycle [Skarstrom, 1960] for separation of a binary feed gas mixture, consisting of:

(a) *Adsorption Step*: Where a binary feed gas mixture to be separated is passed through an adsorber at a super atmospheric pressure level (P^F). The adsorber is pressurized to nearly feed gas pressure level with the product gas prior to start of this step. A purified stream of the less selectively adsorbed component of the feed gas mixture is produced at the adsorber product end which is partially withdrawn as the product gas, a part is used to provide the purge gas to another adsorber undergoing step (c), and the balance is used as the pressurization gas to another adsorber undergoing step (d). The adsorption step is continued until the product gas purity level (average) starts to deviate from the specified value.

(b) *Depressurization Step*: At the end of the adsorption step, the adsorber is depressurized to nearly ambient pressure level (P^D) by withdrawing gas from the adsorber in a direction countercurrent to that of feed gas flow. This gas is rejected.

(c) *Purge Step*: The adsorber is then purged countercurrently using a part of the product gas being produced by another adsorber undergoing step (a) by introducing the gas at pressure (P^P) through the product end. The effluent gas through the feed end during this step is also rejected.

(d) *Pressurization Step*: Finally, the adsorber is pressurized to a pressure level of $\sim P^F$ by using a part of the product gas being produced by another adsorber undergoing step (a) by introducing the gas through the product end.

The cycle then repeats starting from step (a) of the process. A four column system (parallel) can be used to operate the cycle with continuous feed gas introduction and product gas withdrawal and by maintaining the durations of each step equal. Each column carries out one step of the process at any given time.

The conservation equations used in this work to describe each of the process steps are [Sircar, 1991a]:

Component i mass balance:

$$\left\{\frac{\partial}{\partial t}[\rho_g \varepsilon y_i]\right\}_z = -\left\{\frac{\partial}{\partial z}[Q y_i]\right\}_t - \rho_s \left(\frac{\partial n_i}{\partial t}\right)_z \qquad i = 1, 2 \qquad (1)$$

Heat balance:

$$\left\{\frac{\partial}{\partial t}[(\rho_g \varepsilon C_g + \rho_s C_s)(T - T_o)]\right\}_z = -\left\{\frac{\partial}{\partial z}[Q C_g (T - T_o)]\right\}_t + \sum_i \rho_s q_i \left(\frac{\partial n_i}{\partial t}\right)_z \qquad (2)$$

Momentum balance:

$$-\left(\frac{\partial P}{\partial z}\right)_t = \beta(\bar{\varepsilon}, P, y_i, T, Q, d_p) \qquad (3)$$

z is the column distance from the feed gas end. The total column length is L. t is elapsed time from the beginning of a step. t_s is the duration of the step. n_i and y_i are respectively, the specific amount adsorbed and gas phase mole fraction of component i at distance z and time t. Q is the total molar flux through the adsorption column (based on empty cross sectional area) at z and t. P and T are the total gas pressure

and adsorbent (and gas) temperature at z and t. T_o is a reference temperature. ρ_g is the gas density at P and T. q_i is the isosteric heat of adsorption of component i at a loading of n_i. C_g is the molar specific heat of the gas mixture at P, T and y_i. ρ_s and C_s are, respectively, the bulk density and heat capacity of the adsorbent. ε is the helium void fraction of the packed column while $\bar{\varepsilon}$ is the intersticial void fraction. d_p is the adsorbent particle diameter. β represents the transient pressure drop in the column at z and t in a functional notation.

The key assumptions in writing Eqs. (1)–(3) are: (i) instantaneous thermal equilibrium between the gas and solid phases within the adsorber, (ii) perfect column adiabaticity, (iii) absence of radial distribution of mass and heat, and (iv) absence of axial dispersion of mass and heat. We further assumed that the gas phase is ideal [$\rho_g = P/RT$], that the molar specific heat of each gaseous component is a cubic in temperature, and that the transient column pressure drop is given by the Ergun equation [Ergun, 1952]:

$$\beta = \frac{150\mu Q(1-\bar{\varepsilon})^2}{\rho_g (d_p)^2 (\bar{\varepsilon})^3} + \frac{1.75 Q^2 (1-\bar{\varepsilon})}{\rho_g (d_p)(\bar{\varepsilon})^3} \qquad (4)$$

Solution Procedure

To solve the process model equations we used a proprietary software package called SIMPAC, which is an acronym for Simulator for Packed Bed Adsorption Cycles [Hartzog, et.al., 1992]. The governing PDE's are discretized in space using biased upwind differencing with flux correction and the resulting system of time dependent, explicit, first order ordinary differential equations (ODE's) are solved using the LSODES sparse solver from ODEPACK [Hindmarsh, 1983] with the backwards difference option for stiff systems.

Since all four columns of the process were identical and were subjected to the exact same operational steps in a sequential manner, SIMPAC used only one column and associated tanks (simple accumulators) in order to simulate the multi-bed process. For steps where there was direct communication between columns (steps a, c and d), the properties of the exit streams from a column (P, T and y_i) were saved as a function of time and used as the appropriately timed inlet stream to another column. This approach significantly saved computational time.

The initial column conditions (y_i, T and n_i as functions of z^*) at the start ($t = 0$) of each step of the PSA process were assumed to be identical to those at the end ($t = t_s$) of the preceding step after the first cycle of operation. The assumed column conditions for the first cycle are described later. The boundary conditions for each step of the process were fixed as below:

(a) *Adsorption Step*—The feed gas flow rate (Q^F), pressure (P^F), temperature (T^F), and composition (y_i^F) at the column entrance ($z^* = 0$) were held constant during this step. The effluent ($z^* = 1$) gas flow rate was manipulated during this step so that the pressure drop in the column was less than 1.0 atmosphere.

(b) *Depressurization Step*—The flow rate at $z^* = 1$ was fixed to be equal to zero (closed end) and the flow rate at $z^* = 0$ was manipulated so that the column pressure reduces to a near ambient pressure level at time $t = t_s$.

(c) *Purge Step*—The purge gas entrance flow rate and pressure at $z^* = 1$ were maintained at constant values while its composition and temperature varied with time according to those of the effluent gas from a companion column undergoing step (a) which was partly used as purge gas. The purge gas inlet pressure (P^P) was controlled in such a way that the effluent gas ($z^* = 0$) during this step was at ambient pressure.

(d) *Pressurization Step*—The flow rate at $z^* = 0$ was fixed to be equal to zero (closed end) and the flow rate at $z^* = 1$ was manipulated so that the column pressure increased to approximately feed gas pressure level (P^F) at time $t = t_s$. The temperature and composition of the inlet gas ($z^* = 1$) varied with time according to those of the effluent gas from a companion column undergoing step (a) which was partly used as pressurization gas.

For a binary system, there are five state variables (two vapor phase component densities, two solid phase loadings, and one temperature) per spatial node. Hence using N spatial nodes, a system of $5N$ equations must be solved for each step of the process. Note that the molar flux, Q, can be solved analytically from the Ergun equation given the temperature and vapor densities. The appropriate number of nodes was found by increasing the number until no change was observed in performance.

In each simulation, 51 spatial nodes were utilized so that a total of 255 initial value ODE's were solved for each processing step of the cycle. A relative and absolute error tolerance of 1×10^{-6} was specified for each normalized state variable and the maximum integration step-size was limited to five seconds. The

sparstity pattern and Jacobian of the system equations were determined numerically. On an IBM RS/6000 model 550 workstation with a nominal rating of 25.6 MFLOPS, one complete cycle required about 68 CPU seconds. Each simulation started at the beginning of the adsorption step.

The initial conditions utilized depended on whether the run was the very first or a subsequent one. For the first base case simulation, the temperature and pressure profiles were assumed uniform and equal to the respective feed values, while the initial C_2H_4 vapor mole fraction was assumed to decrease linearly from the feed value of 0.20 to 0.0001 at the product end. The solid phase was then assumed to be in equilibrium with the corresponding vapor. About 300 cycles of operation were required before steady state was achieved. All subsequent simulations used the profiles saved at the end of the repressurization step of a previous run as its initial condition, thereby expediting convergence to cyclic steady state. Specified product purity was obtained by manipulating the flow rate of the feed, product, depressurization, purge and/or repressurization streams. Since the purge flow is always choked, it was held at an appropriate fixed value for each run. For the other streams, the flow rate was allowed to vary according to standard formulas for gas flow through a valve. Adjustments were made manually to the purge rate and/or to the sizing coefficients of one or more valves after 10 to 15 cycles in order to meet the product purity specification and keep average step pressures at desired levels.

Adsorption System

Separation of a binary ethylene (1) + methane (2) mixture by the Skarstrom PSA cycle was simulated in this work. The feed gas consisted of 20.0 mole % C_2H_4 (y_1^F) and 80.0 mole % CH_4 (y_2^F) at a pressure of 20.5 atmospheres (P^F) and a temperature of 298 K (T^F). A Nuxit charcoal was used as the adsorbent ($\varepsilon = 0.77$, $\rho_s = 30.0$ lbs/ft^3, $C_s = 0.25$ Btu/lb/°F, $\bar{\varepsilon} = 0.40$). The diameters and lengths of each column were, respectively, 2 feet and 10 feet and they contained 942 lbs of carbon each. The duration of each step was fixed at 2.0 minutes.

The process was run to produce a CH_4 enriched product stream containing 99.88 mole % CH_4 at a product gas pressure of at least 19.5 atmospheres. The two key performance variables were CH_4 recovery (lb moles of CH_4 in product/lb mole of CH_4 in feed gas/cycle) and CH_4 productivity (lb moles of methane produced/lb of total adsorbent in the PSA system/day).

Input Variables

Adsorption Equilibria and Heats

The Nuxit charcoal selectively adsorbs C_2H_4 over CH_4. The pure gas adsorption isotherms of both C_2H_4 and CH_4 on the charcoal are very well described by the Toth isotherm equation [Jaroniec and Toth, 1976]:

$$n_i^o = \frac{mb_iP}{[1+(b_iP)^k]^{1/k}} \qquad i = 1,2 \tag{5}$$

n_i^o is the specific equilibrium amount of pure gas i adsorbed at a pressure of P and temperature T. m is the saturation adsorption capacity of the adsorbent (temperature independent). b_i is the pure gas-solid interaction parameter given by

$$b_i = b_i^* e^{q_i^*/RT} \qquad i = 1,2 \tag{6}$$

q_i^* is the isosteric heat of adsorption of pure gas i at the limit of $n_i^o \to 0$ (Henry's Law limit). b_i^* is the limiting value of b_i as $T \to \infty$. R is the gas constant.

$k(\leq 1)$ is an adsorbent heterogeneity parameter which is a function of T. $k = 1$, represents an energetically homogeneous adsorbent where Eq. (5) reduces to the Langmuir model. The energetic heterogeneity of the adsorbent increases as k decreases. The isosteric heat of adsorption of pure gas i (q_i^o) decreases with increasing fraction coverage $\theta_i^o (= n_i^o/m)$ according to the Toth isotherm due to adsorbent heterogeneity as follows [Sircar, 1991b]:

$$q_i^o = q_i^* + \frac{RT^2}{k^2}\left(\frac{dk}{dT}\right)F(\theta_i^o) \qquad i = 1,2 \tag{7}$$

$$F(\theta_i^o) = \frac{[1-(\theta_i^o)^k]\ln[1-(\theta_i^o)^k] + [(\theta_i^o)^k]\ln(\theta_i^o)^k}{[1-(\theta_i^o)^k]} \tag{8}$$

Figures 1 and 2 show the pure gas adsorption isotherms of C_2H_4 and CH_4 on the Nuxit charcoal at, respectively, 293.1 K and 333.1 K. The circles are the experimental isotherms measured by Szepesy and Illes [1963a]. The solid lines are the best fit of the pure gas isotherms by the Toth model. The model adequately describes the data (within ±5%) over a large range of pressure. It also describes the variation in pure gas isosteric heats of adsorption as functions of adsorbate

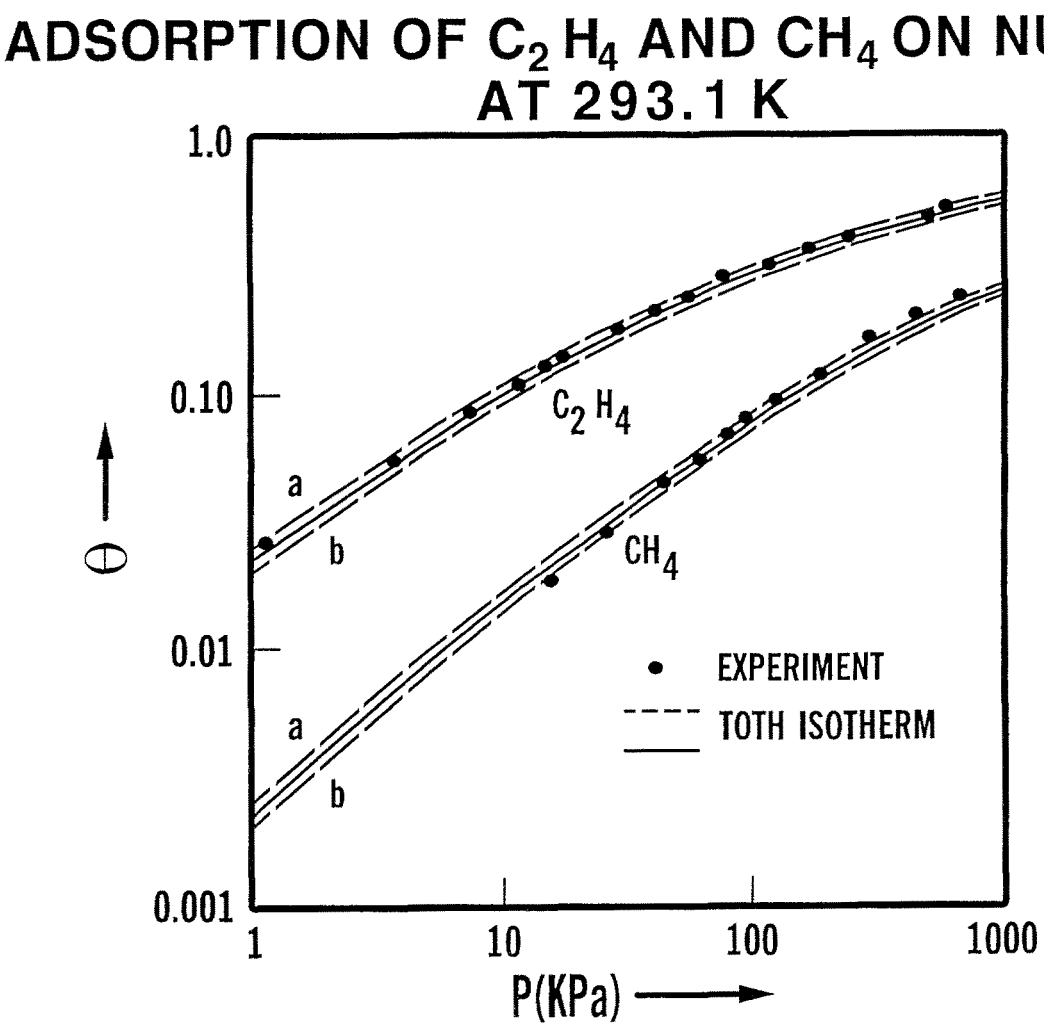

Fig. 1. Pure gas adsorption isotherms of C_2H_4 and CH_4 on Nuxit charcoal at 293 K.

loadings fairly well (within ±1 kcal/mole) as reported earlier [Sircar, 1991b].

Table 1 (base case) summarizes the Toth model parameters for both gases. It may be seen that the same values of m and k at any given temperature can be used to describe both components. This allows the use of the binary Toth isotherm for representing the mixed gas equilibrium adsorption characteristics in a thermodynamically consistent manner:

$$n_i^* = \frac{mb_iPy_i}{[1+(\sum b_iPy_i)^k]^{1/k}} \qquad i=1,2 \qquad (9)$$

n_i^* is the equilibrium specific amount of component i adsorbed at a total gas pressure of P and temperature T when the gas phase mole fraction of component i is y_i. b_i is given by Eq. (6). The Henry's Law selectivity (b_1/b_2) for C_2H_4 adsorption over CH_4 at 293.1 K is 15.0.

According to the Toth isotherm, the isosteric heat of adsorption of component i (q_i) from the binary mixture at the fractional adsorbate loading $\theta_i^*(=n_1^*/m)$ of component i is given by [Sircar, 1991b]:

$$q_i = q_i^* + \frac{RT^2}{k^2}\left(\frac{dk}{dT}\right)F(\theta^*) \qquad i=1,2 \qquad (10)$$

where $\theta^*(=\sum_i\theta_i^*)$ is total fractional adsorbate loading at P, T and y_i. $F(\theta^*)$ has the same functionality as in Eq. (8) except that θ_i^o is replaced by θ^*.

The columns 3 and 4 of Table 2 compare the calculations of [Eq. 9 using pure gas parameters of Table 1] binary C_2H_4 (1) + CH_4 (2) adsorption isotherms on Nuxit charcoal with experimentally mea-

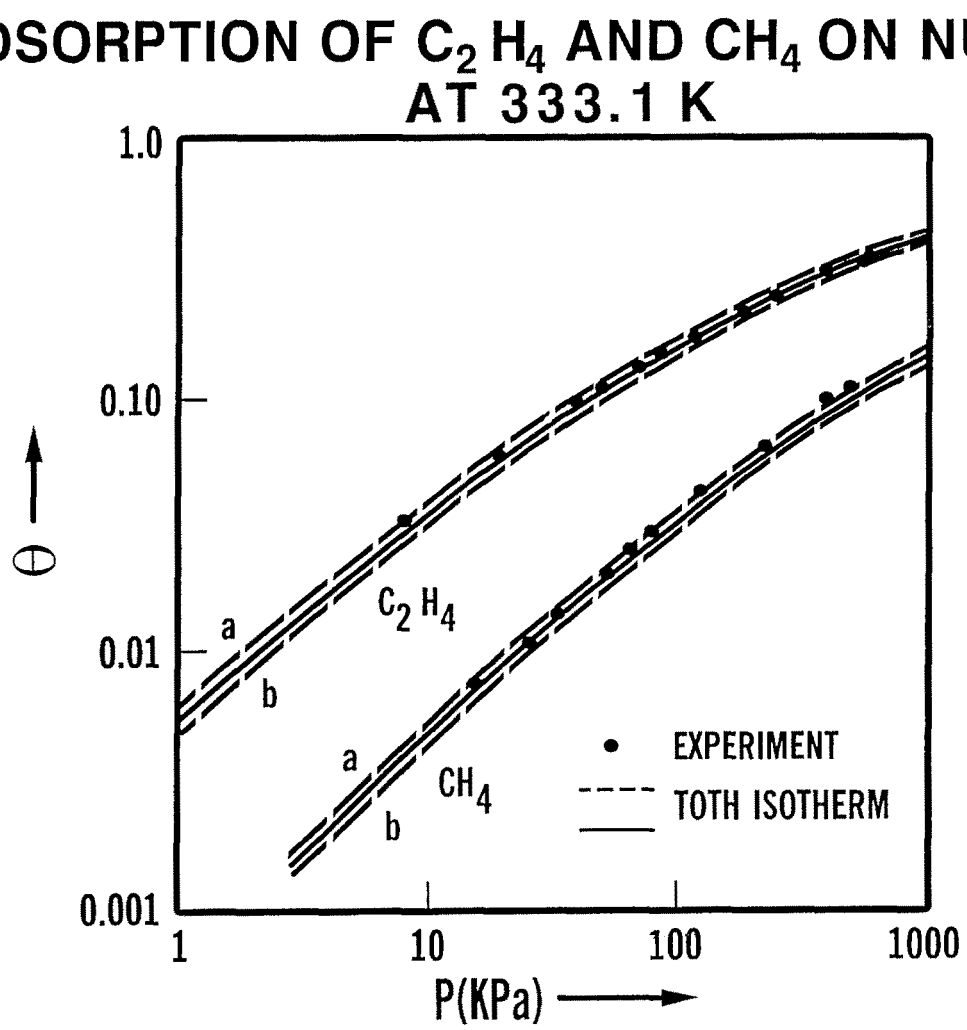

Fig. 2. Pure gas adsorption isotherms of C_2H_4 and CH_4 on Nuxit charcoal at 333 K.

Table 1. Toth model parameters for pure C_2H_4 and CH_4 adsorption on Nuxit charcoal.

	Base Case		Case I		Case II	
	C_2H_4	CH_4	C_2H_4	CH_4	C_2H_4	CH_4
m, (mol/kg)	11.0	11.0	11.0	11.0	11.0	11.0
b_i^*, $(kPa)^{-1}$	7.802×10^{-9}	7.602×10^{-9}	1.562×10^{-9}	1.522×10^{-9}	39.240×10^{-9}	38.230×10^{-9}
q_i^*, (kcal/mole)	9.122	7.560	10.122	8.560	8.122	6.560
k (293 K)	0.34	0.34	0.34	0.34	0.34	0.34
k (333 K)	0.40	0.40	0.40	0.40	0.40	0.40
dk/dT $(K)^{-1}$	0.0015	0.0015	0.0015	0.0015	0.0015	0.0015

sured isotherms (columns 1 and 2) at a total gas pressure of 99.2 kPa and a temperature of 293.1 K. The binary experimental data were reported by Szepesy and Illes [1963b]. The average difference between experimental and calculated θ_1^* values is less than $\pm 3.0\%$ and that for θ_2^* values is less than $\pm 12.0\%$. This kind of error is considered to be very reasonable in predicting equilibrium binary gas adsorption isotherms from pure com-

Table 2. Binary gas adsorption of $C_2H_4(1)+CH_4(2)$ mixture on Nuxit charcoal at 293 K (P = 99.2 kPa).*

	Experiment		Base case		Case I		Case II	
y_1	θ_1^*	θ_2^*	θ_1^*	θ_2^*	θ_1^*	θ_2^*	θ_1^*	θ_2^*
0.1100	0.0766	0.0442	0.0770	0.0415	0.0815	0.0438	0.0735	0.0393
0.1120	0.0837	0.0429	0.0780	0.0412	0.0825	0.0435	0.0739	0.0391
0.2920	0.1464	0.0256	0.1431	0.0231	0.1503	0.0242	0.1364	0.0221
0.3030	0.1387	0.0278	0.1460	0.0224	0.1534	0.0234	0.1394	0.0214
0.5070	0.1940	0.0146	0.1912	0.0124	0.2000	0.0129	0.1831	0.0119
0.5340	0.2000	0.0130	0.1961	0.0114	0.2051	0.0119	0.1879	0.0109
0.7310	0.2312	0.0069	0.2269	0.0056	0.2367	0.0058	0.2179	0.0053
			avg error ±3%	avg error ±12%	avg error ±4%	avg error ±8%	avg error ±6%	avg error ±16%

*Average error={[(calculated)− (experimental)]/[experimental]}×100.

ponent equilibrium adsorption isotherms [Valenzuela and Myers, 1984]. We, therefore, decided to use Eqs. (9) and (10) in conjunction with the parameters of Table 1 to describe the binary equilibrium adsorption and isosteric heats of adsorption for C_2H_4 (1) + CH_4 (2) mixtures on the Nuxit charcoal in our PSA model simulation.

Thus q_i in Eq. (2) is given by Eq. (10) by setting $\theta_i^* = (n_i/m)$ where n_i is the transient specific adsorbate loading of component i in the column at z and t. The limiting Henry's Law isosteric heats of adsorption (q_i^*) of C_2H_4 and CH_4 on the Nuxit charcoal are, respectively, 9.122 and 7.560 kcal/mole indicating that both components are fairly strongly adsorbed by the carbon. It also follows that thermal effects in the column during the adsorption and desorption steps of the process will be pronounced.

Adsorption Kinetics

The linear driving force (LDF) model was chosen to describe the transient adsorption kinetics in the column for both gases [see Eq. 2]:

$$\left(\frac{\partial n_i}{\partial t}\right)_z = k_i[n_i^* - n_i] \qquad i = 1, 2 \qquad (11)$$

n_i is the local specific adsorbate loading of component i in the column at z and t. n_i^* is the corresponding equilibrium specific adsorbate loading at the prevailing gas phase P, T and y_i at z and t. n_i^* is given by Eq. (9). k_i is the over-all gas to solid adsorptive mass transfer coefficient for component i. It was treated as a model variable in the simulation.

For the sake of simplicity, we assumed that k_i is the same for both components and they are independent of n_i and T. Furthermore, we neglected any cross coefficients for describing the over-all adsorptive mass transfer for the components in the LDF model. These assumptions were deliberately made in order to avoid too much complication in the model simulation, although these factors can be very important if adsorptive mass transfer has significant effect on the process performance [Sircar, 1991a].

Process Simulation Results

Base Case

The base case run was made by using the equilibrium adsorption parameters of Table 1 and k_i values of 0.5, 1.0 and 5.0 (seconds)$^{-1}$. The differences in the process performance were very small indicating that these values of k_i variables were large enough to cause local gas-solid adsorption equilibrium in the column. Column 1 in Table 3 summarizes the key process performance characteristics obtained by the simulator using $k_i = 0.5$ (seconds)$^{-1}$. CH_4 recovery was only 28.4% at a purity of 99.88 mole %, while CH_4 productivity was 0.195 lb mols/lb of total carbon in the PSA system/day. The ratio of purge gas quantity (P) to feed gas quantity (F) per cycle evaluated as actual volumes at the inlet P and T conditions of these steps was 2.38 in order to produce the specified product purity. The average purge gas pressure (P^P) was 1.3 atmospheres. The theoretical minimum (P/F) ratio for this case was 1.065 [$1 + P^P/P^F$], which was needed to make the process work [Skarstrom, 1960]. Thus, about 2.25 times more purge gas above the minimum was needed in order to produce 99.88 mole % CH_4 product. This difference can be explained by examining the gas phase composition, adsorbate loading and

Table 3. PSA performance sensitivity to error in heats of adsorption.*

	Base Case	Case I		Case II	
			difference		difference
CH_4 purity (mole %)	99.87	99.88	–	99.88	–
CH_4 recovery (%)	28.40	22.06	−22.3%	36.17	+27.4%
CH_4 productivity (1b moles/1b of carbon/day)	0.195	0.140	−28.1%	0.287	+46.9%
P/F	2.38	3.54	+48.7%	1.95	−18.0%

*Difference = {[(case) − (base case)]/[base case]} × 100.

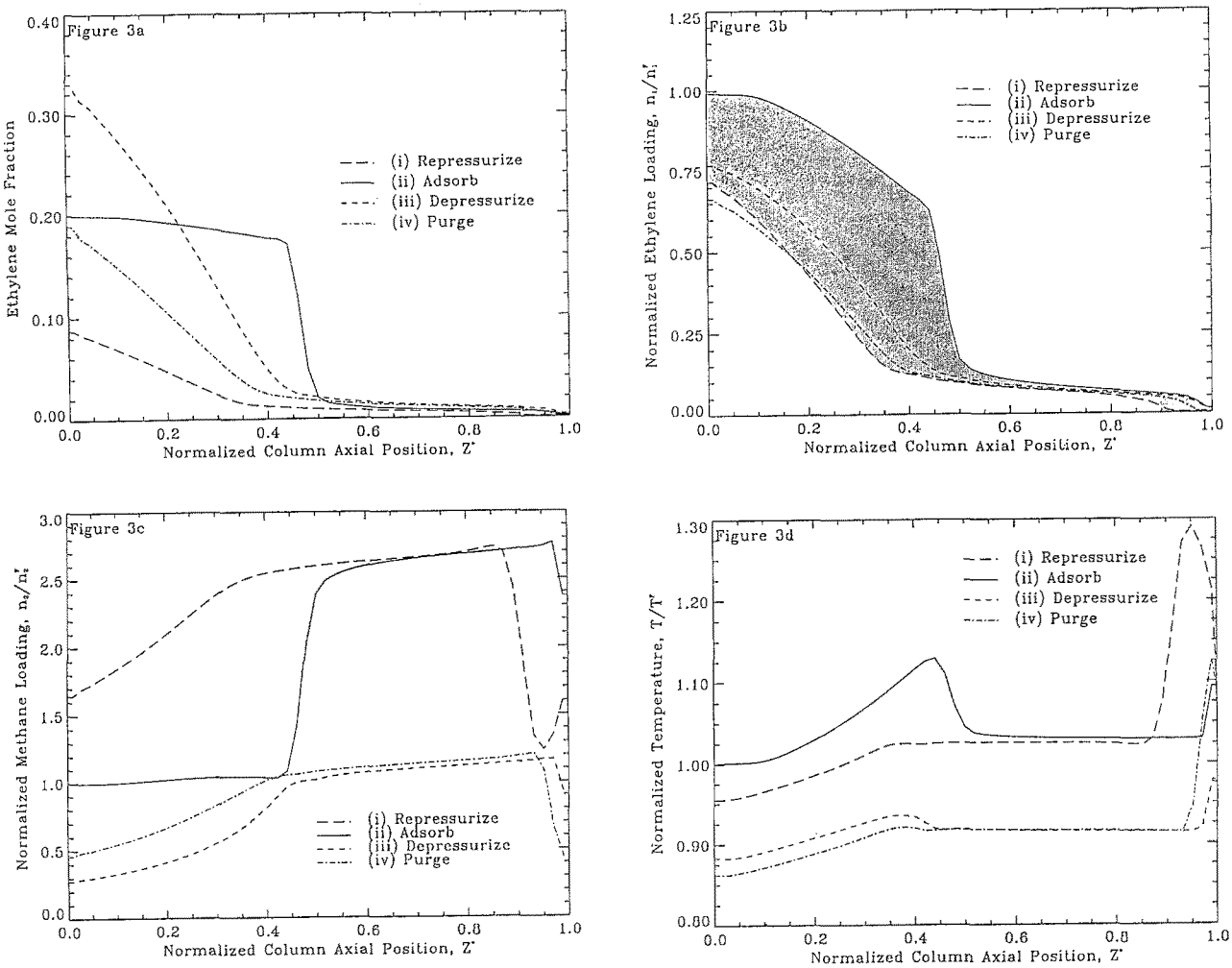

Fig. 3. Simulated gas composition, adsorbate loadings and temperature profiles in column for the base case (Table 1), $k_i = 0.5$ (seconds)$^{-1}$.

temperature profiles within the column during the execution of the process steps.

Figures 3(a–d) respectively, show the gas phase composition of C_2H_4 (y_1), the normalized adsorbate loadings of C_2H_4 ($n_1/n_1{}^F$), the normalized adsorbate loadings of CH_4 ($n_2/n_2{}^F$), and the normalized column temperature (T/T^F) as functions of normalized column distance ($z^* = z/L$) at the end of each step of the cycle after cyclic steady state operation was achieved. Curves (i)–(iv) in these figures describe the profiles

in the column at the end of steps (d), (a), (b) and (c) of the process, respectively. The curve (i) in Fig. 3a shows that C_2H_4 is present in almost the entire length of the column at the end of the pressurization step except at the CH_4 product end ($z^* > 0.9$). The residual C_2H_4 is, however, more concentrated at the feed end ($z^* < 0.4$). Curve (i) of Fig. 3b shows that the actual residual amount of C_2H_4 adsorbed in the column is fairly large at the end of the pressurization step. The CH_4 loading at the end of the pressurization step, given by curve (i) in Fig. 3c, shows that it is largest in the middle section of the column ($0.4 < z^* < 0.9$) where it forms a plateau. The CH_4 loading gradually decreases in the section ($0 < z^* < 0.4$) where the C_2H_4 is concentrated (due to its higher selectivity). However, there is a sharp decrease in the CH_4 loading in the region of ($z^* > 0.9$). This dramatic change is due to the fact that a large amount of heat is generated by CH_4 adsorption during the pressurization step at the CH_4 product end because that end is practically free of C_2H_4, which creates a large CH_4 adsorption capacity. The heat remains stored at that end without travelling far into the column. Furthermore, the inlet pressurization gas is hot because a part of the hot effluent gas from the adsorption step (Fig. 3d) is used as the pressurization gas. Consequently, the curve (i) of Fig. 3d shows a striking rise of temperature at the CH_4 product end at the end of the pressurization step. The temperature rises to about 384 K (111°C) which causes the CH_4 adsorption capacity to be low even though its partial pressure in that region is very high. The temperature profile goes through a maximum and then drops as $z^* \rightarrow 1$ because of cooling caused by the incoming CH_4 gas for pressurization. The gas phase CH_4 composition in the column section described by ($0.4 < z^* \leq 1$) increases very slowly reaching a CH_4 purity of 99.88 + mole % only near the product end.

Curve (i) in Fig. 3d also shows that at the end of the pressurization step the column temperature rises roughly linearly from a minimum of 286 K (13.0°C) at the blocked feed end ($z^* = 0$) to 307 K (34.0°C) at $z^* = 0.4$ where a plateau begins. This plateau extends to about $z^* = 0.9$ and corresponds to the plateau in the CH_4 loading profile, curve (i) of Fig. 3c. During pressurization the temperature along the entire length of the column rose as can be seen by comparing curves (i) and (iv).

Curves (i) and (iv) of Figs. 3a and 3b furthermore show that the C_2H_4 breakthrough front is pushed back towards the feed end, albeit small, during the pressurization step. The C_2H_4 gas phase composition profile from $z^* = 0$ to $z^* = 0.4$ changes substantially [curves 3a (i)] compared to that at the end of purge step [Fig. 3a (iv)]. However, the change in the corresponding C_2H_4 adsorbate loading profile [Curves 3b(i) and 3b(iv)] is rather small.

At the end of the adsorption step, the primary C_2H_4 mass transfer zone [curves 3a(ii) and 3b(ii)] has penetrated only about half way through the column while the effluent gas average CH_4 purity has reached 99.88 mole %. This behavior is caused by the residual C_2H_4 profile at the start of the step [curves 3a(i) and 3b(i)]. Fresh C_2H_4 from feed is adsorbed producing a CH_4 rich stream which displaces residual adsorbed C_2H_4 and spreads the C_2H_4 loading towards the product end. Consequently, breakthrough of C_2H_4 occurs long before the main feed C_2H_4 mass transfer zone has a chance to reach the product end. Also during the adsorption step, the temperature rises everywhere except near the product end as can be seen by comparing curves 3d(i) and 3d(ii). The temperature increase coincides with the adsorption of fresh C_2H_4 and readsorption of displaced residual C_2H_4. At the product end, the thermal peak created during the pressurization step is pushed out of the column thereby lowering the temperature in this region. Some of the hot effluent gas is collected as product but a substantial portion is used to purge and repressurize the other beds.

During the depressurization step (b), both C_2H_4 and CH_4 are desorbed from the column. Consequently, C_2H_4 and CH_4 loadings go down in the entire length of the column [Fig. 3b (iii) and 3c (iii)]. The mole fraction of C_2H_4 in the gas phase goes up [Fig. 3a (iii)] at all values of z^*. However, the C_2H_4 profile at the end of step (b) shows that C_2H_4 decreases rapidly from about 0.33 at the feed end ($z^* = 0$) to about 0.05 in the section ($0 < z^* < 0.4$) and then it decreases slowly to near zero at $z^* = 1.0$. The column temperature decreases over the entire column length [Fig. 3d (iii)] during this step because of the endothermic nature of desorption.

The purge step further reduces both the C_2H_4 vapor concentration and solid loading over the entire length of the column [curves 3a(iv) and 3b(iv)], but the movement is rather small even though a relatively large quantity of purge is used. This behavior is caused by the high selectivity of C_2H_4 over CH_4 and the high strength (heat) of adsorption of C_2H_4. These factors make desorption of C_2H_4 by purging with CH_4 difficult as discussed by Sircar and Kumar (1985). The temperature [curve 3d(iv)] decreases over most of the column during this step, except at the product end, which is heated

by the incoming purge gas. The lowest temperature of 258 K (−15.0°C) occurs at the feed end. The cooling during purge, as during depressurization, is caused by the adsorbent losing its sensible heat in order to supply the heat of desorption.

In contrast to the C_2H_4 loading, the CH_4 loading increases everywhere, except near the product end, during the purge step. This result is due to the very high concentration of CH_4 in the purge gas and the readsorption of residual CH_4 displaced from near the product end by the stripping action of the hot inlet gas.

This cycle is very interesting in that the first half of the column adsorbs and desorbs most of the feed gas C_2H_4 while the small forward and backward movement of the leading edge of the C_2H_4 front near the product end provides the high purity CH_4 product. The small but essential movement of C_2H_4 at the product end is caused by the large volume of product used as purge and repressurization. The shaded area in Fig. 3b gives the C_2H_4 net working capacity.

The simulation reveals the complexity of the dynamics of the ad(de)sorption steps within an adiabatic adsorption column when the thermal effects are pronounced, even for a simple PSA cycle like Skarstrom's. Many subtle nuances in the dynamics (particularly those created by the temperature changes in the column) may not be intuitive. They, however, play a very important role in the overall separation performance of the process. Consequently, the need for developing a detailed model of the PSA process and verification of model calculations using actual performance data from a process development unit are absolutely necessary to guarantee design specifications.

PSA Performance Sensitivity to Input Variables

The base case study shows that the gas phase C_2H_4 mole fraction can vary (at least in sections) between 0.0012 (product specification) to 0.35 (feed gas at 0.20), the column pressure can vary between 1.0 to 20.0 atmospheres (feed gas pressure), and the column temperature can vary from −15°C to +110°C (feed gas at 25°C) during the operation of the cycle. These changes were governed only by the equilibrium adsorption characteristics of C_2H_4–CH_4 mixture for the base case because local gas-solid adsorption equilibrium was achieved due to high value chosen for the k_i. Consequently, the accuracy of the equilibrium model parameters (m, b_i^*, q_i^* and k) in Eqs. (5), (6) and (9) are critical for evaluating the process performance. The most critical parameters are q_i^* and b_i^* because they determine the value of b_i at any given T (Eq. 6) which subsequently determine the selectivity (b_1/b_2) as a function of T and the isosteric heats of adsorption of the mixture (q_i) as functions of adsorbate loadings (Eq. 10).

We found that the pure gas adsorption isotherms of C_2H_4 and CH_4 at 293 and 333 K (Figs. 1 and 2) can be adequately described by simultaneously increasing the base case q_i^* values for C_2H_4 and CH_4 by +1.0 kcal/mole or by simultaneously decreasing them by −1.0 kcal/mole using appropriate changes in b_i^* values while keeping m and k values intact (see Table 1). These changes maintain the selectivity of adsorption of C_2H_4 at 293°K the same as the base case $(b_1/b_2 = 15.0)$, and give the same temperature coefficient of selectivity [constant $(q_1^* - q_2^*)$].

The dashed lines a and b in Figs. (1) and (2) describe the pure gas isotherms for C_2H_4 and CH_4 according to Eqs. (5) and (6) using the higher and lower values of q_i^*, respectively. The average error spread is within ±5% which is well within typical experimental errors. The columns under Cases I and II of Table 2 show the corresponding calculations of binary isotherms. The average errors in calculation of θ_1^* is within +6% and that for θ_2^* is within ±16%. These are also within typical experimental errors. In fact, an error of ±1.0 kcal/mole in the isosteric heats of adsorption at the Henry's Law region which constitute only ±11% error for q_i^* and ±13% error for q_2^* for the system under consideration is well within the experimental error [Sircar, 1991b]. It will be shown in the following that these kinds of errors in the input equilibrium parameters can cause significant difference in the performance of the above described PSA process.

We ran SIMPAC simulations of the process using the equilibrium parameters given by Cases I and II of Table 1 and using k_i values of 0.5 (seconds)$^{-1}$. The product purity of 99.88 mole % CH_4 was maintained. Figures 4(a–d) and 5(a–d) show the corresponding cyclic steady state gas phase composition, adsorbate loadings and temperature profiles in the column, respectively, for the higher (Case I) and lower (Case II) q_i^* values. It may be seen that these profiles are qualitatively very similar to those for the base case but the absolute values of the key variables in the profiles change substantially. For example, the ranges of temperature changes in the column are between −18° and +140°C for Case I and between −12° and +94°C for Case II. The corresponding maximum C_2H_4 gas phase mole fractions at the end of the depressurization step are respectively 0.30 and 0.38. A major difference in

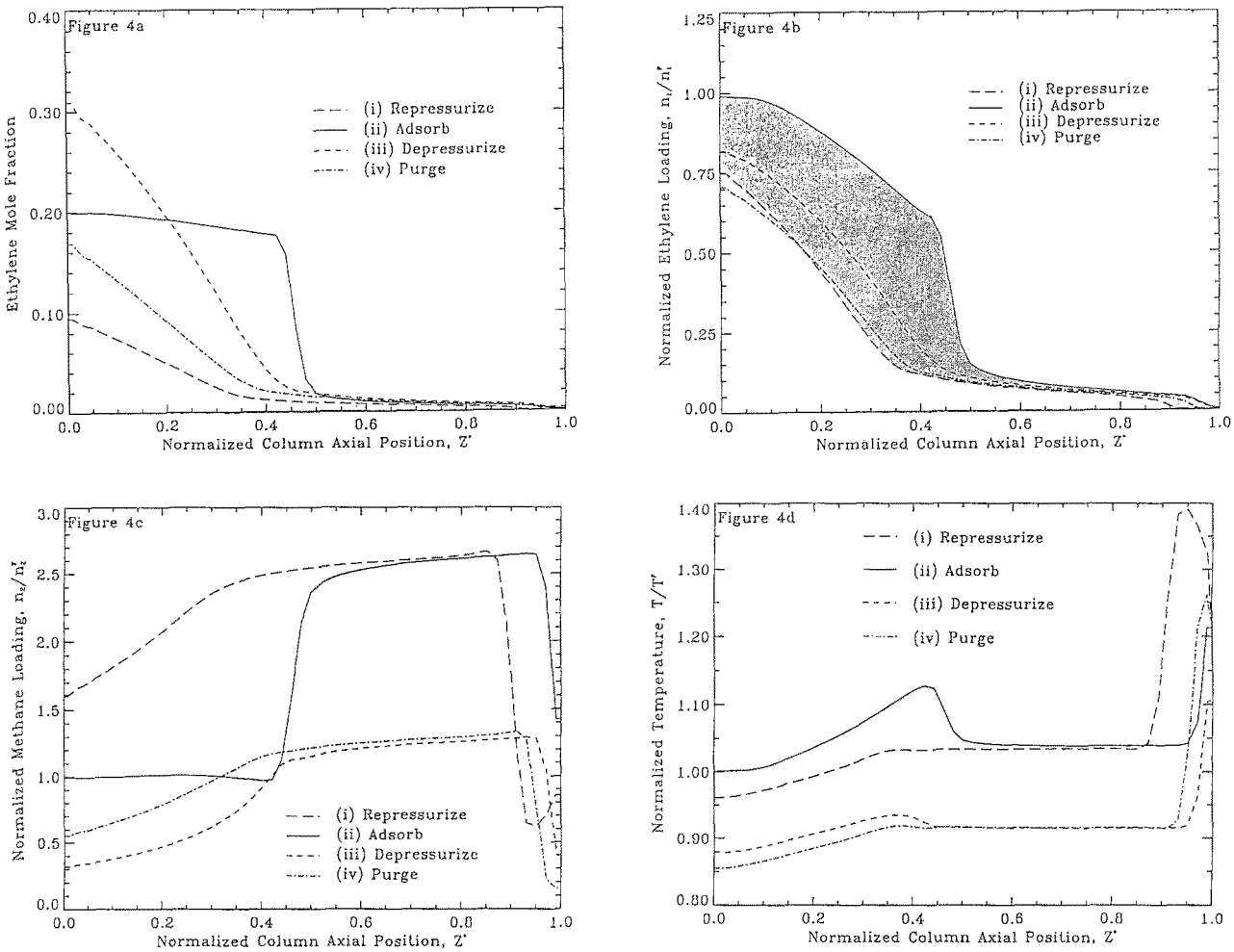

Fig. 4. Simulated gas composition, adsorbate loadings and temperature profiles in column for Case I (Table 1), $k_i = 0.5$ (seconds)$^{-1}$.

the internal column dynamics for these cases is the back and forward movement of the leading edge of the C_2H_4 front at the product end. For Case I the movement is smaller than that for the base case while for Case II it is larger than that for the base case. The second major difference is the net working adsorption capacity for C_2H_4 in the column (shaded areas in Figs. 4b and 5b). Case I yields a much smaller C_2H_4 working capacity than the base case. Case II gives a larger C_2H_4 working capacity than the base case. These differences are primarily caused by the higher and lower heats of adsorption of the two cases albeit small compared to the base case.

The net results of these differences are summarized in Table 3. CH_4 recovery decreases by 22% for Case I but increases by 27% for Case II compared to that for the base case. CH_4 productivity decreases by 28% for Case I while it increases by 47% for Case II compared to that for the base case. Furthermore, a 49% increase in (P/F) ratio (Case I) and a 18% decrease in that ratio (Case II) are needed compared to the base case in order to maintain a CH_4 product purity of 99.88 mole %.

These kinds of uncertainty in estimating the performance of the PSA process by model calculations are not practically acceptable. It is critical that the temperature profiles in the column be simulated as correctly as possible and the effects of temperature on the multicomponent equilibrium and kinetic adsorptive properties be accurately known over the entire range of conditions prevailing in the adsorber so that PSA process models can be reliably used for process design and optimization.

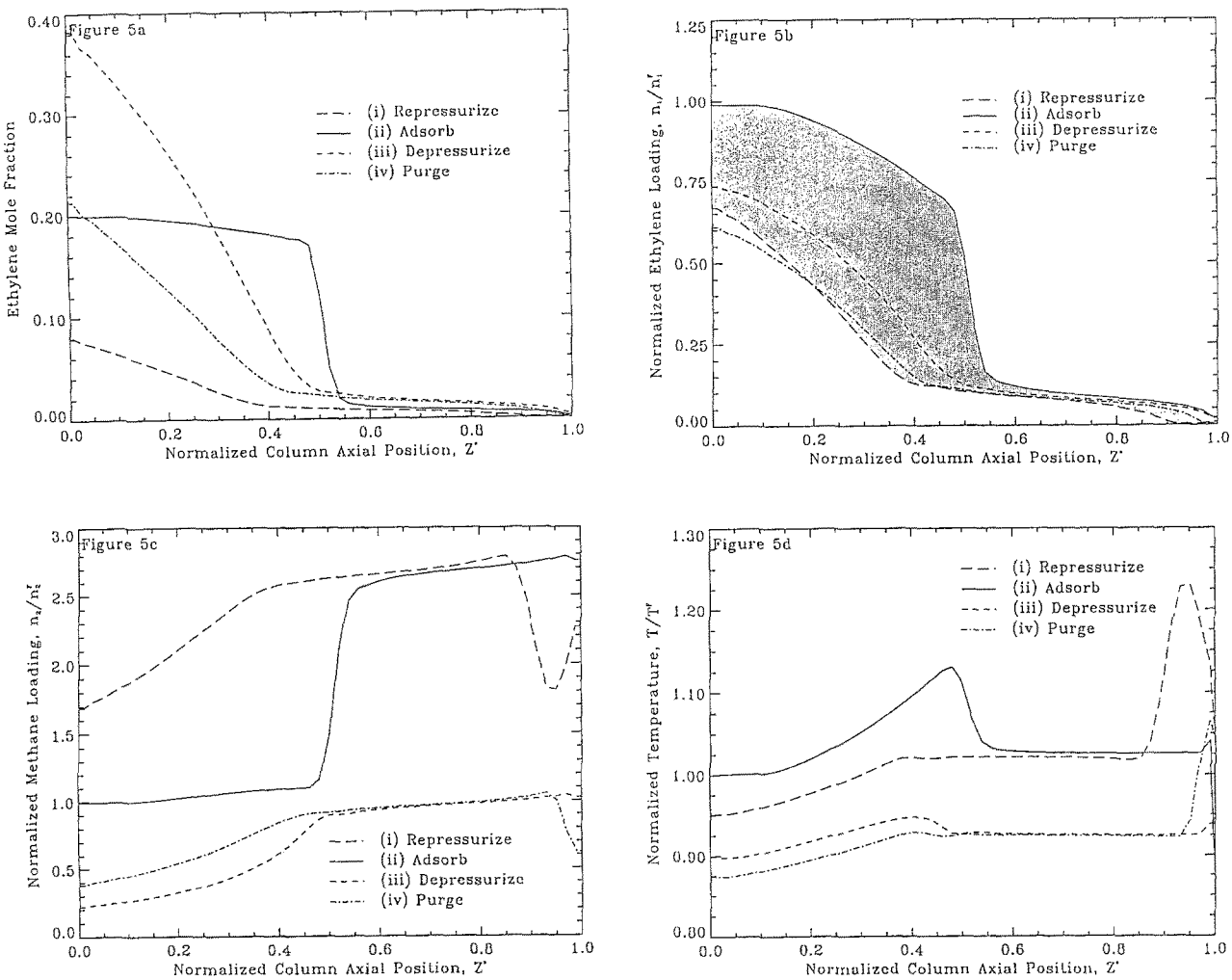

Fig. 5. Simulated gas composition, adsorbate loadings and temperature profiles in column for Case II (Table 1), $k_i = 0.5$ (seconds)$^{-1}$.

Effect of Uncertainty in Kinetic Parameters

SIMPAC simulations were run using k_i values of 0.25, 0.10 and 0.05 (seconds)$^{-1}$ in conjunction with the equilibrium characteristics of the base case (Table 1). All these cases exhibited substantial departure from the local equilibrium base case performance. Table 4 summarizes the process performance for these runs and Figs. 6(a–d) show the column profiles for the case when k_i is 0.1 (seconds)$^{-1}$. The CH_4 product purity was maintained at 99.83–99.88% for these runs. It may be seen from Table 4 that both CH_4 recovery and productivity go down when the adsorbates have larger mass transfer resistances. At the same time, P/F substantially increases as the k_i values go down, in order to maintain the CH_4 product purity. A comparison between Figs. 3 and 6 show that the dynamic profiles within the column are again qualitatively similar. However, the C_2H_4 adsorption fronts at the middle of the column and at the product end are much less sharper for the non-equilibrium case as expected [Figs. 3b(ii) and 6b(ii)]. The net C_2H_4 working capacity is also much smaller when $k_i = 0.10$ compared to that for $k_i = 0.5$.

The data of Table 4 are replotted in Fig. 7 as fractional changes in CH_4 recovery and productivity (compared to those for the base case) as functions of k_i. It shows that the change of these performance properties for a small change in k_i can be large when $k_i < 0.2$ (seconds)$^{-1}$. Thus, the tolerance of error in the estimation of k_i values can be small when adsorbate mass transfer resistances are important, in order to obtain practically acceptable design performance.

Table 4. PSA performance sensitivity to error in mass transfer coefficient.*

	k_i (seconds)$^{-1}$			
	$k_i = 0.5$ (Base Case)	$k_i = 0.25$	$k_i = 0.10$	$k_i = 0.05$
CH_4 purity (mole %)	99.87	99.88	99.86	99.83
CH_4 recovery (%)	28.40	26.49 (−6.7%)	21.73 (−23.5%)	12.23 (−56.9%)
CH_4 productivity (lb moles/lb carbon/day)	0.195	0.178 (−8.9%)	0.139 (−29.1%)	0.081 (−58.8%)
P/F	2.38	2.47 (+3.8%)	2.79 (+17.2%)	5.92 (+148.7%)

*Difference = {[(case) − (base case)]/(base case)} × 100.

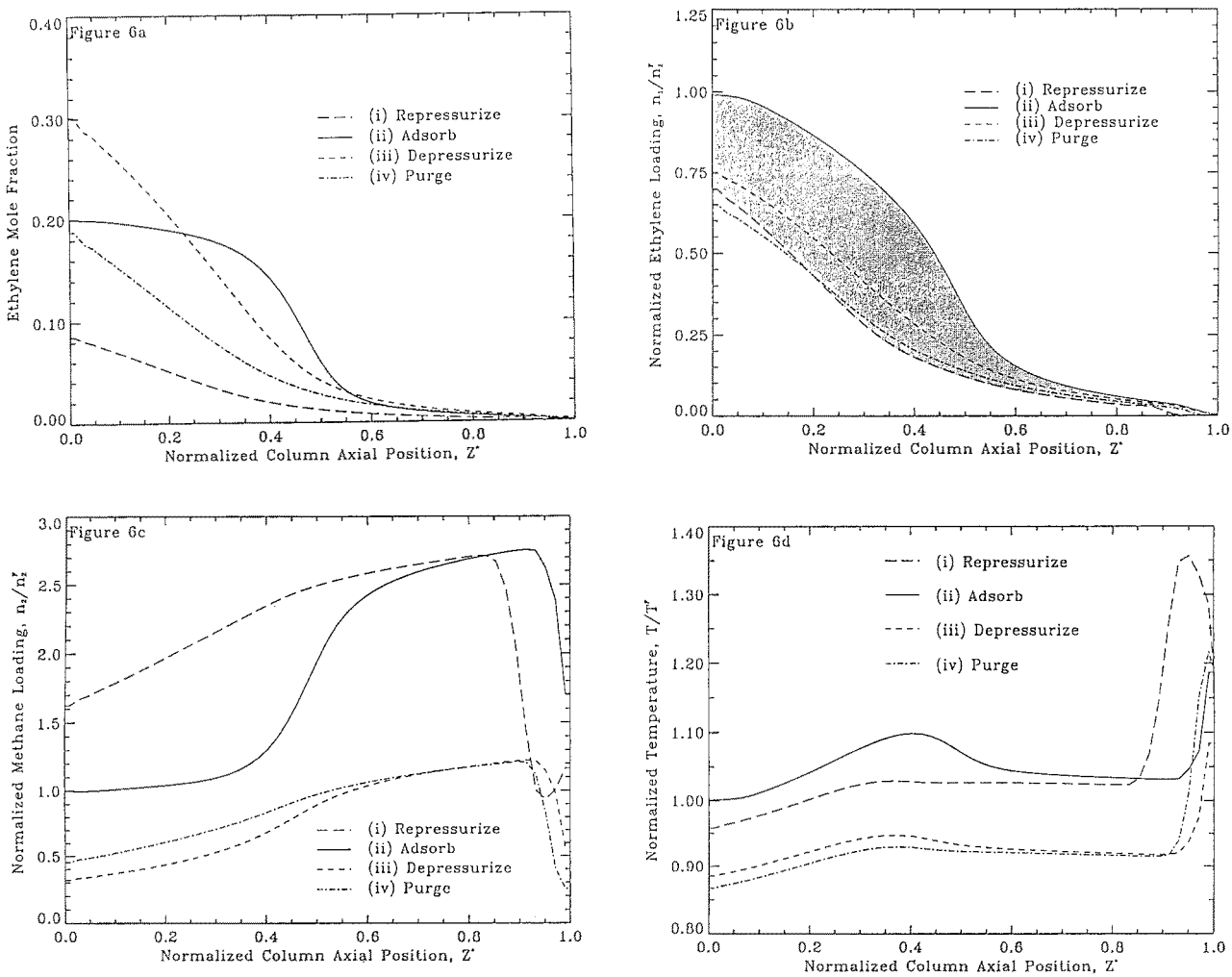

Fig. 6. Simulated gas composition, adsorbate loadings and temperature profiles in column for base case (Table 1), $k_i = 0.1$ (seconds)$^{-1}$.

The simplest method to directly obtain k_i for pure gases is by the non-isothermal differential uptake measurement using gravimetric tests. The adsorbent is subjected to a differential change in gas phase pressure and the weight change of the adsorbent (fractional uptake, f) is monitored as a function of time (t) until equilibrium is attained. The non-isothermal uptake of a pure gas using the LDF model [Eq. 11] can be

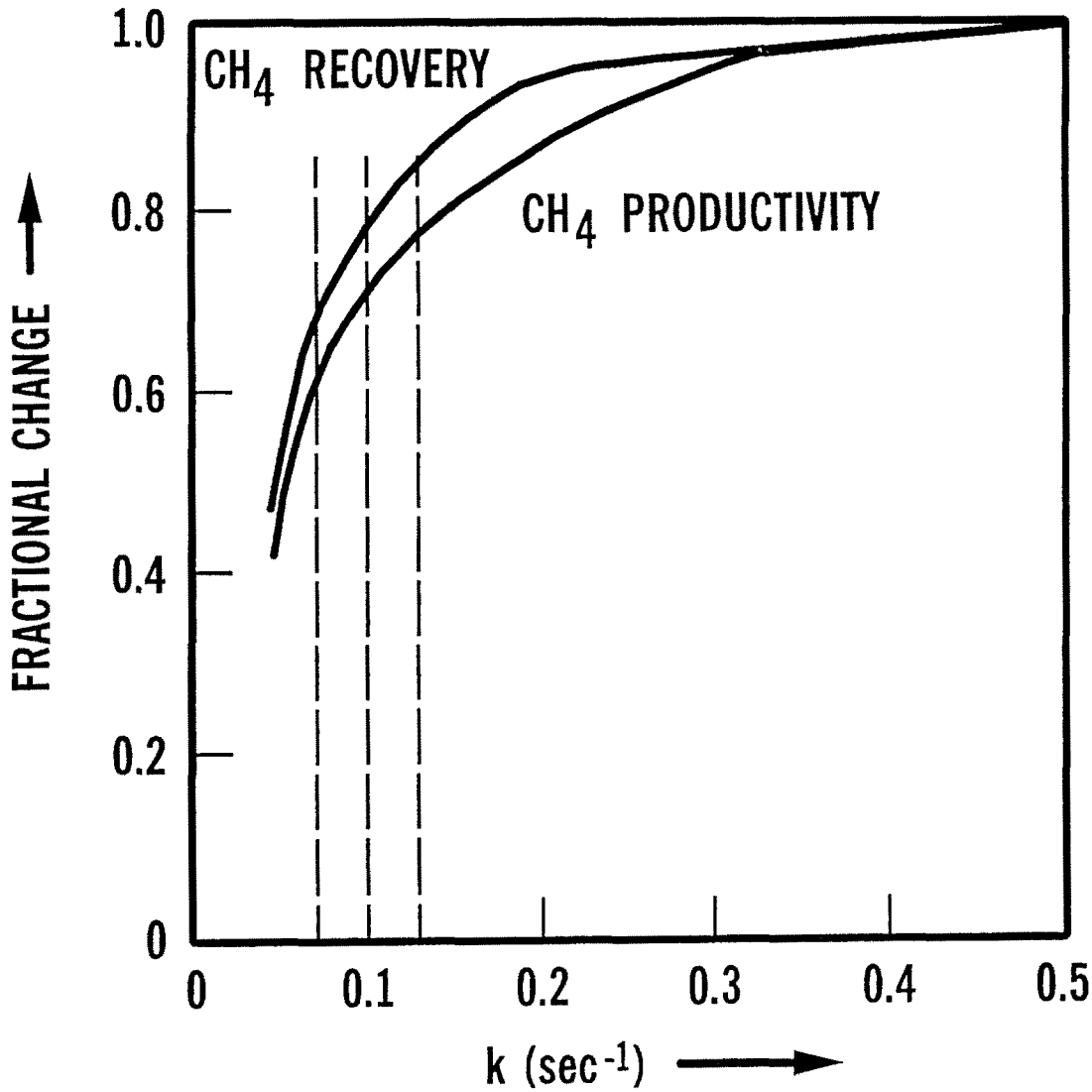

Fig. 7. Effects of adsorptive mass transfer coefficient on CH_4 recovery and productivity by Skarstrom PSA process for making 99.88 mole % methane product.

described analytically as [Sircar, 1983]:

$$1 - f(t) = \frac{-(\beta\alpha^2)}{(1-\beta\alpha^2)}\left[e^{\nu t} - \left\{\frac{e^{-k_i(1-\alpha\beta)t}}{(\beta\alpha^2)}\right\}\right] \quad (12)$$

$$\nu = -0.5k_i\left[(1-\beta+\lambda) - \sqrt{(1-\beta+\lambda)^2 - 4\lambda}\right] \quad (13)$$

$$\beta = \frac{-m[q(\theta)]^2[\theta(1-\theta)^k]}{C_s R T_o^2};$$

$$\lambda = \frac{h \bullet a}{C_s \bullet k_i}; \quad \alpha = \frac{k_i}{k_i + \nu}$$

β, λ and α are dimensionless quantities. β defines the differential heat effects during the uptake process for the Toth isotherm. m and k are Toth parameters, θ is the fractional adsorbate loading at the test condition $q(\theta)$ is the corresponding isosteric heat of adsorption [Eq. 7]. C_s is the adsorbent heat capacity and T_o is the initial and final temperature during the uptake test. λ is the ratio of the time constants for heat transfer from the adsorbent and mass transfer into the adsorbent. $(h \bullet a)$ is the product of characteristic external heat transfer coefficient (h) from the adsorbent of transfer area (a).

The circles in Fig. 8 show the calculated uptake of pure C_2H_4 by Nuxit charcoal in a differential test at 293 K $(= T_o)$ using the equilibrium properties (base case, Table 1) at $\theta = 0.05$. The k_i for this case is

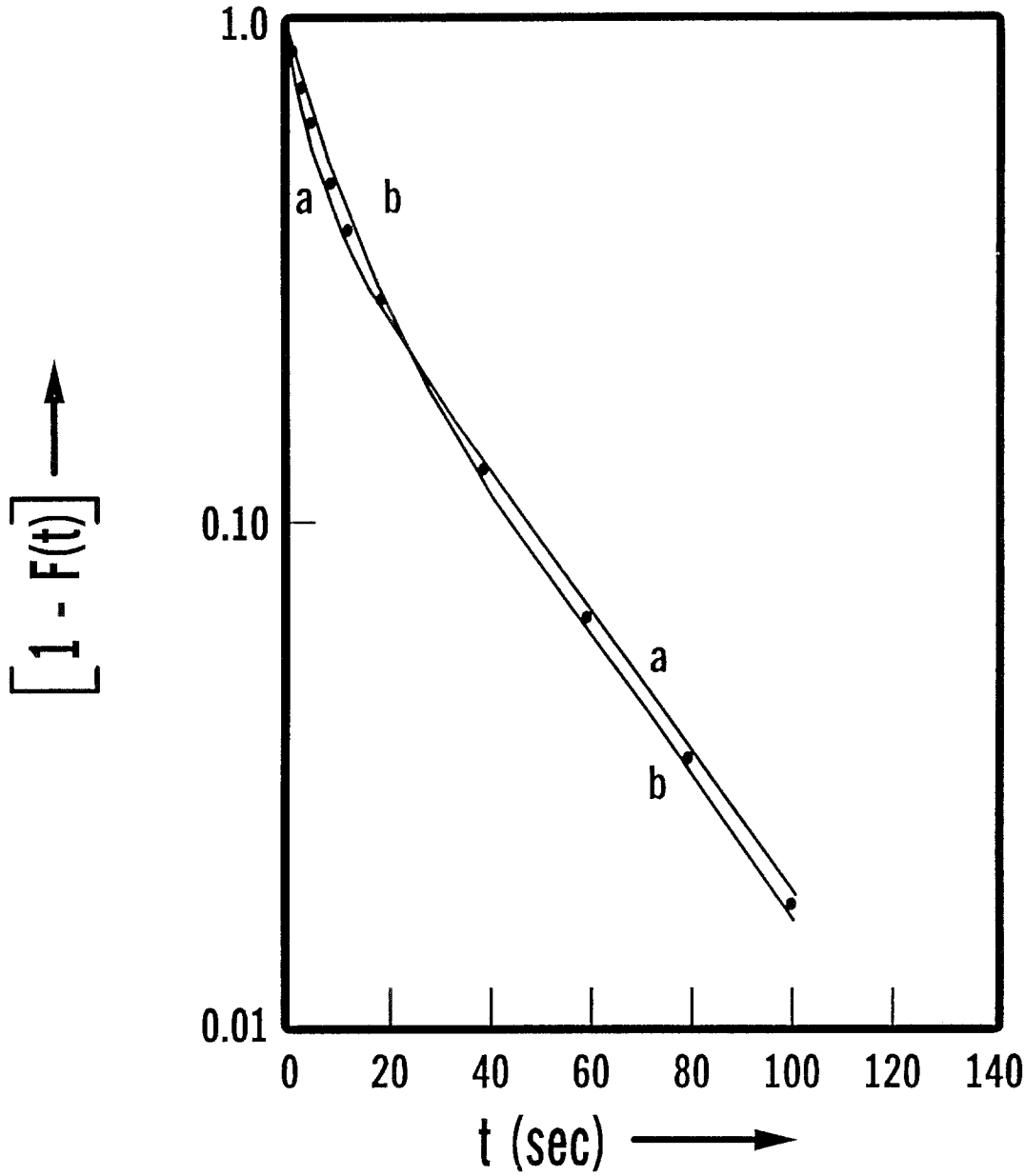

Fig. 8. Uptake curves for C_2H_4 by a non-isothermal differential kinetic test.

0.1 (seconds)$^{-1}$, $C_s = 0.25$ cal/g/K, and the quantity (ha/C_s) is equal to 0.05 (seconds)$^{-1}$ which is typical for such tests. 98.0% equilibrium uptake is reached in about 100 seconds. Assuming that the uncertainty in estimating q_i^* for C_2H_4 is given by the cases I and II of Table 1, we refitted the uptake curve (generated by using the base case equilibrium parameters) of Fig. 8 with modified values of β in Eqs. (12) and (13) using q_i^* values of 10.122 and 8.122 kcal/mole and new k_i values. Other parameters were kept constant. The dashed lines in Fig. 8 show the results. Curves (*a*) and (*b*) correspond to cases I and II, respectively. The average difference between the circles and the dashed lines is less than $\pm 10\%$ which is well within the errors in a typical kinetic test data. The k_i values were, respectively, 0.125 and 0.085 (seconds)$^{-1}$ for curves *a* and *b*. Thus,

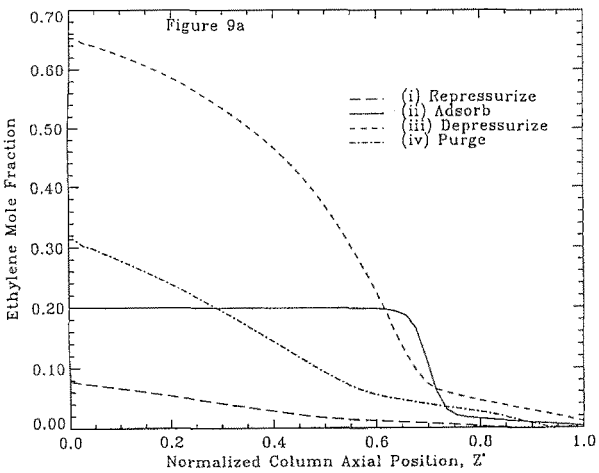

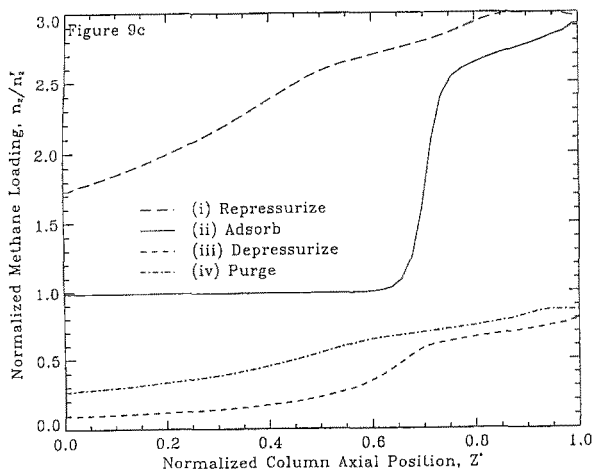

a ±20% error in estimating k_i value from the uptake rate measurement can be common.

It may be seen from Fig. 7 that a ±20% error in estimating k_i values (around $k_i = 0.1$) for the adsorbates can introduce a spread of 0.72–0.82 and a spread of 0.65–0.75 in calculating fractional changes in CH_4 recovery and productivity, respectively. The spreads will be much larger if k_i is less than 0.1. Obviously, the errors will be much smaller when the conditions of local-equilibrium operation is approached. It should be noted that the curves of Fig. 7 were generated using the q_i^* values of the base case. The combinations ($k_i = 0.125$, $q_i^* = 10.122$, $q_2^* = 8.560$) and ($k_i = 0.085$, $q_1^* = 8.122$, $q_2^* = 6.560$) will result in much larger spreads in process performance than those shown by Fig. 7.

It may be concluded that the individual component adsorptive mass transfer coefficients must also be known very accurately when adsorption kinetics are

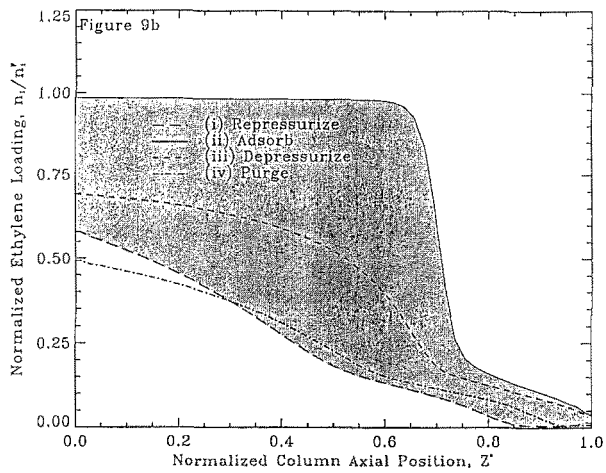

Fig. 9. Simulated gas composition and adsorbate loading profiles in column for isothermal operation.

slow, in order to obtain a practically acceptable process design by simulation.

Sensitivity of CH_4 Product Purity

SIMPAC runs were made using base case input variables for making 99.98 (Case A) and 99.77 (Case B) mole % CH_4 products from the same feed gas. Table 5 shows the simulation results. The CH_4 recovery went down by ~12% and the CH_4 productivity was reduced by ~10% when the mole fraction of CH_4 product was increased by only 0.0011 from the base case. This shows the extreme sensitivity of the process performance when purer product is made. On the other hand, Table 5 shows that the process performance is not changed much when the CH_4 product mole fraction is reduced by 0.001 from the base case. Consequently, it may be concluded that the tolerance of errors in the input variables to the PSA model can be critical when a pure product is required. Experimental verification of the process performance will be a must for such a case.

Two Extreme Situations

Isothermal Case

The performance of the above described process under the condition of isothermal column operation was studied by setting ($q_i^* = 0$, $dk/dT = 0$) but using the same b_i and k values [Eq. 9] and k_i values [Eq. 11] as those

Table 5. PSA product purity and process performance*.

	Base Case	Case A	Case B
CH_4 purity (mole %)	99.87	99.98	99.77
CH_4 recovery (%)	28.40	25.07 (−11.7%)	28.95 (+1.9%)
CH_4 productivity (lb moles/lb carbon/day)	0.195	0.177 (−9.2%)	0.193 (−1.0%)
P/F	2.38	3.12 (+31.1%)	2.03 (+14.7%)

*Difference = {[(case) − (base case)]/(base case)} × 100.

Table 6. PSA process performance under extreme conditions.

	Base Case	Isothermal	Constant Heats
CH_4 purity (mole %)	99.87	99.87	99.88
CH_4 recovery (%)	28.40	60.16 (+111.8%)	18.92 (−33.3%)
CH_4 productivity (lb moles/lb carbon/day)	0.195	0.828 (+324.6%)	0.125 (−36.1%)
P/F	2.380	1.48 (−37.8%)	5.0 (+110.0%)

*Difference = {[(case) − (base case)]/(base case)} × 100.

of the base case at the feed gas conditions. Figure 9(a–c) show the dynamic profiles for this case. Figures 9a and b show that (1) the penetration of the C_2H_4 zone into the column is much deeper ($0 < z* < 0.7$) during adsorption step of the process, (2) the backward and forward movement of the leading edge of the product end C_2H_4 front is much larger, and (3) the net C_2H_4 working capacity of the column is much bigger for this case. Table 6 compares the performance of the isothermal case with that of the base case. A dramatic 110% and 326% improvement in CH_4 recovery and productivity, respectively, can be achieved by isothermal operation. The (P/F) ratio needed for this case to obtain a 99.87 mole % CH_4 product purity is only 1.48 which is nearly 40% more than the theoretical minimum. Since, isothermal operation cannot be achieved in practical adsorbers, evaluation of the process performance using such an assumption can be extremely misleading (optimistic).

Constant Isosteric Heats Case

The base case of the present study includes the effect of variation of isosteric heats of adsorption of the components with variations in adsorbate loadings [Eqs. (7), (8) and (10)], which is a characteristic of the adsorbent heterogeneity. Nuxit charcoal is a fairly heterogeneous adsorbent for adsorption of C_2H_4 and CH_4 as indicated by the small k values (Table 1). Failure to account for this effect can also lead to very misleading results. A SIMPAC run was made by assuming that $(dk/dT = 0)$ which removes the effect of heterogeneity on the isosteric heats of adsorption. They remain constant $(= q_i^*)$ and independent of θ_i (or θ_i^0) for the mixture or pure gas adsorption. Such assumptions have often been made inadvertently in the published literature by approximately describing the adsorption isotherms using energetically homogeneous isotherm models.

Table 6 summarizes the process performance for this case. The CH_4 recovery and productivity are reduced by 33% and 36% from the base case values, respectively. This is caused by much more pronounced thermal effects in the column due to the assumption of high q_i^* values at all adsorbate loading. The (P/F) ratio to obtain 99.88% CH_4 product gas in this case is 5.0. Clearly such assumptions can lead to very pessimistic process design even as a first pass screening effort.

Conclusions

The quality of simulation of a PSA process performance using a mathematical process model largely depends on the detailedness of the model and the accuracy of the input variables such as multicomponent adsorption equilibria, heats and kinetics. These vari-

ables must be known over the entire ranges of pressure, temperature and gas compositions prevailing inside the adsorber during all steps of the cyclic process. Some of the key findings of this study are:

(i) It is crucial that the temperature profiles inside the adsorber be simulated accurately during all process steps when the heats of adsorption of the components are moderate to large. Accurate values of isosteric heats of adsorption of the components in the Henry's Law region must be determined and the variation of the isosteric heats as functions of adsorbate loadings for gas mixture adsorption on a heterogeneous adsorbent must be described correctly in order to obtain practically acceptable process performance. A $\pm 10\%$ error in these variables may introduce large errors in simulation.

(ii) It is preferable that multicomponent adsorption equilibria and heats are expressed as analytical functions of pressure, temperature and gas phase compositions or adsorbate loadings at all conditions of operations. The equations for adsorption equilibria should describe the experimental data within $\pm 2\%$.

(iii) The adsorbate mass transfer coefficients play a crucial role in establishing over-all process performance when operating under non-equilibrium conditions. They must be known with an accuracy of better than $\pm 10\%$ when the thermal effects are important because the driving force for mass transfer can be strong functions of local temperatures.

(iv) The sensitivity of the PSA process performance to the errors in input variables becomes amplified when a stringent product gas specification (particularly high purity product) is demanded.

(v) Simplified first pass design assumptions like isothermal operation or constancy of isosteric heats of adsorption for a heterogeneous adsorbent may lead to very optimistic or pessimistic process performance.

(vi) It is recommended that simulated designs be thoroughly verified by actual process performance data before they are used for scale-up or optimization.

Nomenclature

a Specific heat transfer area from adsorbent in differential kinetic test
b_i Interaction parameter of Toth isotherm equation
b_i^* b_i at $T \to \infty$
C_g Molar heat capacity of gas
C_s Heat capacity of adsorbent
d_p Particle diameter
f Fractional uptake in differential kinetic test
F Feed gas quantity per cycle in PSA process
h External heat transfer coefficient in differential kinetic test
k Parameter of Toth isotherm equation
k_i Adsorptive mass transfer coefficient for component i
L Column length
m Saturation adsorption capacity of Toth isotherm equation
n_i Specific amount of component i adsorbed
P Pressure
P/F Purge to feed gas quantity (actual volume)
P^P Purge gas inlet pressure
P^F Feed gas inlet pressure
P^D Final depressurization pressure
Q Superficial molar flux through column
q_i Isosteric heat of adsorption of component i
q_i^* Pure gas isosteric heat of adsorption at Henry's Law region
R Gas constant
t Time
T Temperature
T_o Reference temperature
y Gas phase mole fraction
z Distance in column
z^* z/L

Greek Letters

α Parameter in Eq. (13)
β Parameter in Eq. (13)
λ Parameter in Eq. (13)
ν Parameter in Eq. (13)
μ Gas viscosity
ρ_g Gas density ($= P/RT$)
ρ_s Adsorbent bulk density
θ_i Fractional adsorbate loading for component i ($= n_i/m$)
θ Total fractional adsorbate loading ($= \sum \theta_i$)
ε Total void fraction in column
$\bar{\varepsilon}$ Inter-particle void fraction in column

Superscripts and Subscripts

D Desorption
F Feed gas entrance conditions

P Purge gas entrance conditions
i Component i
$*$ Equilibrium conditions
o Pure gas

References

Ergun, S., "Fluid Flow Through Packed Columns," *Chem. Engr. Prog.*, **48**(2), 89 (1952).

Hindmarsh, A.C., "ODEPACK, A Systematized Collection of ODE Solvers," *Scientific Computing*, R.S. Stepleman et al. (Eds.), North-Holland, Amsterdam, 1983.

Hartzog, D.G., V.G. Fox, R. Kumar, Y.C. Chen, P.A. Houghton, and T. Naheiri, "A Versatile Process Simulator for Adsorptive Separations," paper presented at AIChE Meeting in Miami, Florida, Nov. 1992.

Jaroniec, M. and J. Toth, "Adsorption of Gas Mixtures on Heterogeneous Solid Surfaces: Extension of Toth Isotherm on Adsorption from Gas Mixtures," *J. Colloid Polym. Sci.*, **254**, 643(1976).

Sircar, S., "Linear Driving Force Model for Non-Isothermal Gas Adsorption Kinetics," *J. Chem. Soc. Faraday Trans. I.*, **79**, 785 (1983).

Sircar, S., and R. Kumar, "Equilibrium Theory for Adiabatic Desorption of Bulk Binary Gas Mixture by Purge," *I.&E.C. Proc. Des. Dev.*, **24**, 358 (1985).

Sircar, S., "Pressure Swing Adsorption: Research Needs by Industry," *Fundamentals of Adsorption*, Proceedings of the Engineering Foundation Conference held at Sonthofen, Germany, A.B. Mersmann et al. (Eds.), 815(1991a).

Sircar, S., "Isosteric Heats of Multicomponent Gas Adsorption on Heterogeneous Adsorbents," Langmuir, **7**, 3065 (1991b).

Skarstrom, C.N., "Method and Apparatus for Fractionating Gaseous Mixtures by Adsorption," U.S. Patent 2,944,627 (1960).

Szepesy, L. and V. Illes, "Adsorption of Gases and Gas Mixtures, I," *Acta Chim. Hung.*, **35**, 37 (1963a).

Szepesy, L. and V. Illes, "Adsorption of Gases and Gas Mixtures, III," *Acta Chim. Hung.*, **35**, 245 (1963b).

Valenzuela, D., and A.L. Myers, "Gas Adsorption Equilibria," *Separation and Purification Methods*, **13**, 153 (1984).